Desalination and Water Treatment
www.deswater.com

doi: 10.5004/dwt.2018.22219

110 (2018) 193–208
April

Optimization of the photocatalytic activity of N-doped TiO_2 for the degradation of methyl orange

Mohsen Nasirian[a], Ciro Fernando Bustillo-Lecompte[b,c], Yi Ping Lin[c], Mehrab Mehrvar[c,*]

[a]*Graduate Programs in Environmental Applied Science and Management, Ryerson University, 350 Victoria Street, Toronto, ON, Canada M5B 2K3, email: mohsen.nasirian@ryerson.ca*
[b]*School of Occupational and Public Health, Ryerson University, 350 Victoria Street, Toronto, ON, Canada M5B 2K3, email: cbustill@ryerson.ca*
[c]*Department of Chemical Engineering, Ryerson University, 350 Victoria Street, Toronto, ON, Canada M5B 2K3, Tel. +1 (416) 979-5000 Ext. 6555; Fax: + 1 (416) 979-5083; emails: mmehrvar@ryerson.ca (M. Mehrvar), ylin@ryerson.ca (Y.P. Lin)*

Received 22 October 2017; Accepted 18 March 2018

ABSTRACT

Methyl orange, a well-known detrimental azo dye, is treated by N-doped TiO_2 photocatalyst synthesized by the simple and effective annealing method. In this study, the effects of light intensity in terms of irradiance by the number of lamps, photon energy and radiation sources, the initial concentration of total organic carbon (TOC), and pH on the degradation efficiency of methyl orange are investigated. A four-factor Box–Behnken design along with response surface methodology is used to maximize the removal of TOC and color. Statistical models are developed to predict both color and TOC removals as response variables. In all cases, the light intensity and TOC concentration cross-factor interaction with the light wavelength is intensified when the latter is at the lowest range value while pH does not require adjustments. Maximum TOC and color removals of 96.11% and 98.18%, respectively, were achieved at the optimum operating conditions of light intensity in terms of five lamps, light wavelength of 418 nm (visible light range), initial TOC concentration of 10.54 mg/L, and pH of 6.66. The model was validated by an additional experiment at the optimal operating conditions. The agreement between experimental values and model predictions demonstrate the proposed models could effectively describe the degradation of azo dyes by photocatalysis using the N-doped TiO_2 composite under visible light.

Keywords: N-TiO_2; Photocatalytic doping; Azo dyes; Response surface methodology; Process optimization; Advanced oxidation processes

1. Introduction

The textile manufacturing industry produces large volumes of industrial wastewater containing azo dyes, with potential adverse effects on the aquatic life when released into water bodies. Chemical reactions taking place in the wastewater, such as oxidation or hydrolysis, can produce toxic and carcinogenic by-products that are detrimental to the environment. Nearly 20% of the global dye production is being released as textile wastewater [1–5].

As azo dyes possess high resistance to biodegradation, advanced oxidation processes (AOPs) are an attractive alternative to conventional treatment methods for the removal of dyes from industrial wastewater because of the ability of these methods to mineralize the target contaminants, avoiding the formation of hazardous by-products [2–9]. AOPs are based on the production of hydroxyl radicals (•OH) to oxidize almost all organic materials in wastewater effluents due to its high oxidation potential of 2.8 eV [5,10–18]. Photocatalysis is one of the diverse types of AOPs, and TiO_2, among all photocatalysts, has been widely studied as one of the most promising photocatalysts for environmental treatment due to its superior properties, including high reactivity,

* Corresponding author.

non-toxicity, high physicochemical stability, and low price [1,6,19,20]. However, the application of TiO_2 is limited by its large band gap energy of 3.2 eV, which restricts the use of solar irradiation and increases the production costs, and the high recombination rate of electron–hole pairs, which reduces the photocatalytic activity of TiO_2 [6,19–22].

Recent studies have focused on the construction of two-dimensional (2D) nanosheets and three-dimensional (3D) nanoarrays of photocatalysts and the doping of photocatalysts to improve photocatalytic activity by increasing their specific surface area and enhancing their photoactivities towards the visible light region. Some of these doped photocatalysts include $CdIn_2S_4$/rGO, g-C_3N_4, and N-doped TiO_2 nanosheets [23–29]. Non-metal doping of TiO_2 using B, C, N, S, or F has been considered as an efficient method to increase the specific surface area of TiO_2 and to expand the absorption wavelength of TiO_2 towards the visible-light region. Among all, N-doped TiO_2, with a band gap energy of 2.3 eV, has a high photodegradation efficiency, less expensive than other semiconductors, and mitigates the electron–hole recombination processes [19–22,29–33]. However, the efficiency of a photocatalyst is influenced by several parameters during the photocatalytic reaction. Among all, organic concentration, pH, light intensity, light wavelength, and reaction time have a significant and direct influence on the degradation efficiency of organic pollutants.

On the other hand, AOPs are multifactor systems as a result of the cross-factor interaction of different parameters during the treatment process [13,14]. Therefore, the use of design of experiments (DOEs) is an appropriate approach to identify the influence of factors in the multivariable system in forms of single factors and interaction effects. DOE is also used to overcome the limitations of conventional procedures regarding time and materials required, and subsequently, optimize the variables involved in the response surface methodology (RSM) to attain optimal responses using the minimum number of experiments [13–16,29].

In this study, the effects of the light intensity, wavelength, initial concentration of total organic carbon (TOC), and pH, as well as their interaction on the degradation efficiency of methyl orange were investigated. The DOE was used to find the optimum operating conditions of the photocatalytic treatment of an azo dye by maximizing the TOC and color removals in a methyl orange aqueous solution under visible light. The optimal parametric values for the DOE were obtained using a four-factor Box–Behnken design (BBD) along with RSM. Then, statistical models were developed to predict both percentual removal of TOC and color as process responses. Lastly, the statistical quadratic models were validated in another set of experimental runs at optimum operating conditions.

2. Materials and methods

2.1. Materials and instrumentation

All chemical materials were of analytical grade, purchased, and used as received without additional purification from Sigma-Aldrich (Oakville, ON) and Van Waters and Nat Rogers (VWR) Canada (Mississauga, ON).

Scanning electron microscopy (SEM; JSM-6370LV, JEOL, Calgary, AB) coupled with energy dispersive spectroscopy (EDS; Oxford Instrument Model X-Max-N-80, Concord, MA) was used to characterize both morphology and chemical composition of individual particles. An auto sputter coater (Denton Vacuum Desk IV, Moorestown, NJ) was used for coating samples with a thin layer of gold before analysis by SEM. The specific surface area of the photocatalyst powder was obtained based on the Brunauer, Emmet, and Teller (BET) technique (Nova e-Series 1200, Quantachrome Instruments, Boynton Beach, FL), in which physical adsorption of nitrogen occurred at 77 K. X-ray diffraction (XRD) model PANalytical X'pert PRO (St Laurent, QC) was used to characterize the crystal structure and conversion phase of TiO_2 with the scanning range of 10°–100° (2θ).

The photoactivity of the as-prepared photocatalyst was assessed by measuring the degradation of methyl orange using two different methods. The first method was based on the TOC concentration measured by an automated TOC analyzer (Model Apollo 9000, Teledyne Tekmar, Mason, OH). The second method was based on the measurement of color by an Orbeco-Hellige colorimeter model MC500-Multiparameter (Sarasota, FL, USA). Before analysis either by TOC analyzer or colorimeter, all samples were first centrifuged at 4,000 rpm for 30 min using a centrifuge (Thermo Scientific Heraeus Multifuge X1, Mississauga, ON) followed by filtration using a filter paper (VMR Qualitative 410, Mississauga, ON). All experimental runs and analytical measurements were repeated in triplicates. Thus, the mean values were reported.

2.2. Photocatalyst synthesis

In this study, the annealing method was adopted for the synthesis of nitrogen-doped TiO_2. The annealing method involves the mixing of the TiO_2 powder and the source of non-metal dopant, urea in this case, and then heating and calcining simultaneously the mixture in the furnace to obtain the resultant non-metal doped photocatalyst (N-TiO_2). Different amounts of precursors were used to prepare N-TiO_2 photocatalysts at various mass ratios (0.05–0.35 w:w N-TiO_2). To prepare 0.05 w:w N-TiO_2, 0.107 g of grounded urea was added to 1 g of P25 TiO_2. The content was mixed for 10 min and calcined at 350°C for 3 h. Then, the product was washed with water and ethanol; then it was dried at 105°C in an oven. The annealing method is considerably faster and more straightforward than other doping methods when the required TiO_2 precursor is already available for use [34].

It must be ensured a thorough mixing of the two solids to obtain uniformly doped photocatalyst. Otherwise, a portion of the final product might be made up of only the initial photocatalyst, while the other portion is the doped photocatalyst. The final product of the as-prepared N-TiO_2 consists of a large specific surface area and high photocatalytic activity.

2.3. Experimental setup and procedure

A laboratory-scale batch photoreactor with uniform light distribution was used for the degradation of methyl orange in the presence of as-prepared photocatalysts. The schematic diagram of the experimental setup is presented in Fig. 1. The batch photoreactor was made of a glass container with a total working volume of 3.5 L (Fig. 1(a)) and a lid for holding different irradiation sources (Fig. 1(b)).

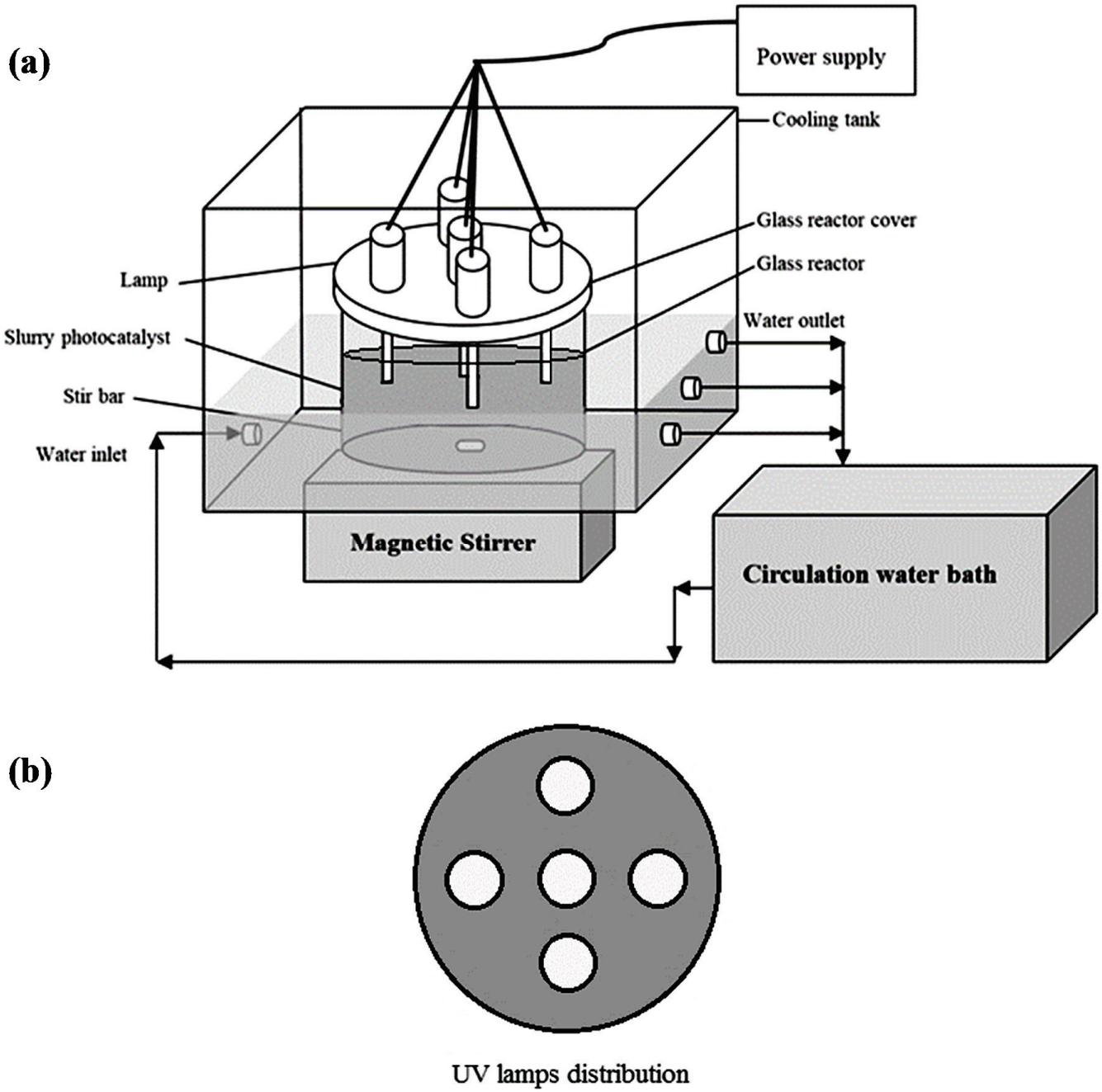

Fig. 1. Schematic diagram of (a) the laboratory-scale batch suspension reactor and (b) the lid for UV lamps distribution.

The irradiation sources were varied depending on the experimental run and included five lamps at centered peak wavelengths of 254, 365, and 476 nm for UV-C (PL-S 9W/TUV-UV Germicide, 110-120V, G23 Base), UV-A (Philips BL PL-S 9W 110-120V, 2P Actinic G23 Base), and Visible (PL-2PIN 9W 110-120V, G23 Base) lights, respectively. All lamps were settled vertically on the top of the reactor.

Before running each experiment, the photocatalyst powder and methyl orange solution were added in the photoreactor. The slurry was stirred under dark for 50 min so that the solution reaches to equilibrium. This equilibrium time was determined and validated by carrying out an experiment for 180 min in dark, where the results showed that an equilibrium was reached after 50 min between the solid and the liquid phases.

The degradation of aqueous methyl orange was performed under continuous stirring using a magnetic stirrer. The exterior of the reactor was covered with aluminum foil to prevent any interference from external light sources and temperature variations. The TOC and color removals were monitored every 30 min for each experiment to measure the degree of mineralization and decolorization of methyl orange, respectively. The temperature of the solution in the main reactor was controlled by a recirculating water

bath (RTE-211, NESLAB Instruments, Inc., Newington, NH). Solutions of 1 N sulfuric acid (H_2SO_4) and 1 N sodium hydroxide (NaOH) were added as required for pH adjustments. The photoactivity of as-prepared photocatalysts was evaluated by the percentual degradation of methyl orange calculated by Eq. (1):

$$\mathrm{TOC}_{\mathrm{removal}}(\%) = (\mathrm{TOC}_{\mathrm{o}} - \mathrm{TOC}) / \mathrm{TOC}_{\mathrm{o}} \times 100 \quad (1)$$

where TOC_o and TOC are the initial and remaining concentrations of TOC, respectively. The photocatalytic degradation of methyl orange was carried out in the presence of N-TiO_2 photocatalysts with different mass ratios of N to TiO_2 (0.05–0.35 w:w N-TiO_2).

2.4. Statistical experimental design

A four-factor BBD with RSM was applied to maximize the percentage of the TOC and color removals. The light wavelength (X_1), initial concentration of TOC (X_2), light intensity in terms of irradiance by the number of lamps (X_3), and pH (X_4) were employed as independent variables (i.e., predictors) while the TOC removal (Y_1) and color removal (Y_2) were considered as dependent variables (i.e., process responses) in the DOE. Accordingly, each studied predictor was coded at three levels (from −1 to +1), as shown in Table 1.

A quadratic model was used to estimate the parametric coefficients of the statistical models by correlating both predictors and responses using the least-squares regression as shown in Eq. (2) [13–16,29]:

$$Y_i = \beta_o + \sum_{i=1}^{k} \beta_i X_i + \sum_{i=1}^{k} \beta_{ii} X_i^2 + \sum_{i=1}^{k-1} \sum_{j=2}^{k} \beta_{ij} X_i X_j + c \quad (2)$$

where β_o, β_i, β_{ii}, and β_{ij} correspond to the constant, linear, quadratic, and cross-factor interaction coefficients, respectively; whereas X_i and X_j represent the predictors, Y_i is the response under evaluation, and k and c are the number of predictors of the model and the residual error term, respectively. The statistical software Design-Expert 10.0.3.1 was employed for the DOE as well as the estimation of the coefficients for each response. The significance of each model equation, individual parameters, and factor interactions was evaluated via analysis of variance (ANOVA) at the confidence interval of 95% (α = 0.05). 2D contour plots and 3D surface responses were obtained with the quadratic models. Additional experimental runs were conducted to validate the quadratic models for the maximum removals of TOC and color at the optimum operating conditions, calculated by the software numerical optimization method.

Table 1
Experimental design and independent variables based on RSM for the optimization of the photocatalytic activity of N-doped TiO_2 in the degradation of methyl orange

Independent variables	Symbol	Range and levels		
		–1	0	1
Light wavelength (nm)	X_1	254	365	476
TOC_o (mg/L)	X_2	10	30	50
Light intensity (number of lamps)	X_3	1	3	5
pH	X_4	5	7	9

On the other hand, the desirability multiple-response approach was utilized to obtain a concurrent objective function to represent all transformed responses by combining the desired ranges for each response as shown in Eq. (3) [14,15,35]:

$$D = \left(Y_1 \times Y_2 \times \ldots \times d_n\right)^{1/n} = \left(\prod_{i=1}^{n} Y_i\right)^{1/n} \quad (3)$$

In this equation, D, Y_i, and n are the desirability term, each evaluated response, and the total number of process responses, respectively. For a simultaneous optimization, each response function requires low and high values for the optimization. Otherwise, if any response is found outside the desirability range, the global desirability becomes equal to zero. In this case, two responses are being optimized: the percent TOC removal (Y_1) and the color removal (Y_2).

3. Results and discussion

3.1. Preliminary studies

Fig. 2 illustrates the degradation of methyl orange in the presence of as-synthesized N-TiO_2 with different mass ratios of nitrogen to TiO_2 after 180 min of UV-A irradiation. Results presented an improvement in photocatalytic degradation of methyl orange as the mass ratio of nitrogen in N-TiO_2 was increased to 0.15 w:w N-TiO_2, where efficiency reached 40.9%. It is concluded that at high concentrations of nitrogen after the optimal value, the surface of TiO_2 photocatalyst became shielded by the nitrogen atoms, and thus, there is less surface available for the absorption of light to trigger the generation of electron and hole for degradation of organics. A similar trend was observed in the specific surface area

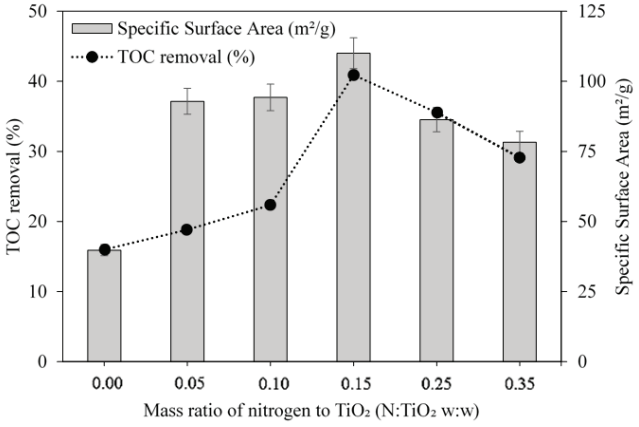

Fig. 2. Degradation of methyl orange by UV-A/N-TiO_2 photocatalyst (500 mg/L) with different mass ratios of nitrogen after 180 min of reaction time, and comparison with the specific surface area of photocatalysts.

of N-TiO_2 photocatalyst. When TiO_2 photocatalyst is doped with nitrogen, both interstitial and substitutional doping can exist [5,6,20].

In the interstitial doping, the dopant is not incorporated into the crystal lattice, it resides between the crystals on an interstitial site, which introduces states in the band gap, but generally, it does not dope the n-type or p-type semiconductors [36]. On the other hand, substitutional doping causes crystal defects and decreases the band gap energy. In other words, when a non-metal species, such as nitrogen with a slightly higher energy level compared with oxygen, is introduced into the TiO_2 lattice, a new mid-gap energy state is generated. This mid-gap energy state holds the potential of absorbing energy from radiation of light at higher wavelengths to produce a significant amount of •OH [20,28,36,37]. Thus, UV radiation excites the electrons in both the valence band and the mid-gap energy level; whereas, visible light can only excite the electrons in the mid-gap energy level [20,36–39].

The specific surface area of photocatalysts with different mass ratios of doped nitrogen was measured using BET technique by adsorption of nitrogen gas at 77 K. Results showed that the N-TiO_2 photocatalyst with the mass ratio of 0.15 w:w N-TiO_2 had the highest specific surface area of 110.01 m^2/g compared with that of bare P25, 39.77 m^2/g, and bare urea, 34.36 m^2/g. By increasing the concentration of doped nitrogen in N-TiO_2 above its optimal value, its specific surface area was decreased. As the specific area of N-TiO_2 is increased, more reaction sites are available, and thus, higher photocatalytic efficiencies in the degradation of methyl orange are achieved. Therefore, the N-TiO_2 photocatalyst with an N:TiO_2 mass ratio of 0.15 w:w was chosen for the statistical experimental design.

3.2. Photocatalyst characterization

Fig. 3(a) illustrates an SEM image of the 0.15 w:w N-TiO_2 photocatalyst, prepared via the annealing method. In this figure, particles have a heterogeneous flat shape variable particle size in the range of 1–10 μm based on the scale. Particles contain light and dark nanoparticles, which are supposed to contain more pores on the surface.

In the EDS elemental analysis of N-TiO_2 photocatalyst, the nitrogen and oxygen peaks are overlapping; therefore, the elemental analysis of N-TiO_2 is not conclusive. This circumstance is caused by the resemblances between nitrogen and oxygen, which present similar characteristic in EDS. Thus, the instrument is not able to adequately separate their elemental peaks. Consequently, XRD and mapping of the N-TiO_2 photocatalyst were used to illustrate the distribution and relative proportion of the compounds and elements over the scanned area, respectively.

Fig. 3(b) shows an XRD diffractogram of the N-doped TiO_2 photocatalyst (0.15 w:w N-TiO_2) prepared using annealing method. The crystalline phase was confirmed by comparing the attained diffractograms with the standard, which present the location of the TiO_2 peaks, based on the Joint Committee on Powder Diffraction Standards (JCPDS-21-1272) databank [40]. Based on the Joint Committee on Powder Diffraction Standards, anatase (JCPDS-21-1272) has a primary peak at 25.4° (2θ), and other anatase peaks are located at 37.8°, 48.0°, and 54.5° related to planes, and rutile (JCPDS-21-1276) has two main peaks, one at 2θ = 27.5° and the other one at 2θ = 36.1°. Rutile may also have another peak at 2θ = 54.4° [40]. P25 has one main peak at 2θ = 25.4° and two other peaks at 2θ = 37.8° and 48.0°, which belong to anatase. Also, it has a peak at 2θ = 27.5° and 36.1°, which belong to rutile.

The diffractogram indicates the presence of both the anatase (2θ = 25.4°, 37.8°, 48.0°, and 54.5°) and the rutile (2θ = 27.5° and 36.1°) forms of TiO_2, and similar to P25 TiO_2 (Fig. 3(c)), it indicates that there was no change in the crystalline phases of TiO_2 in the N-TiO_2 photocatalyst. Thus, the crystal structures

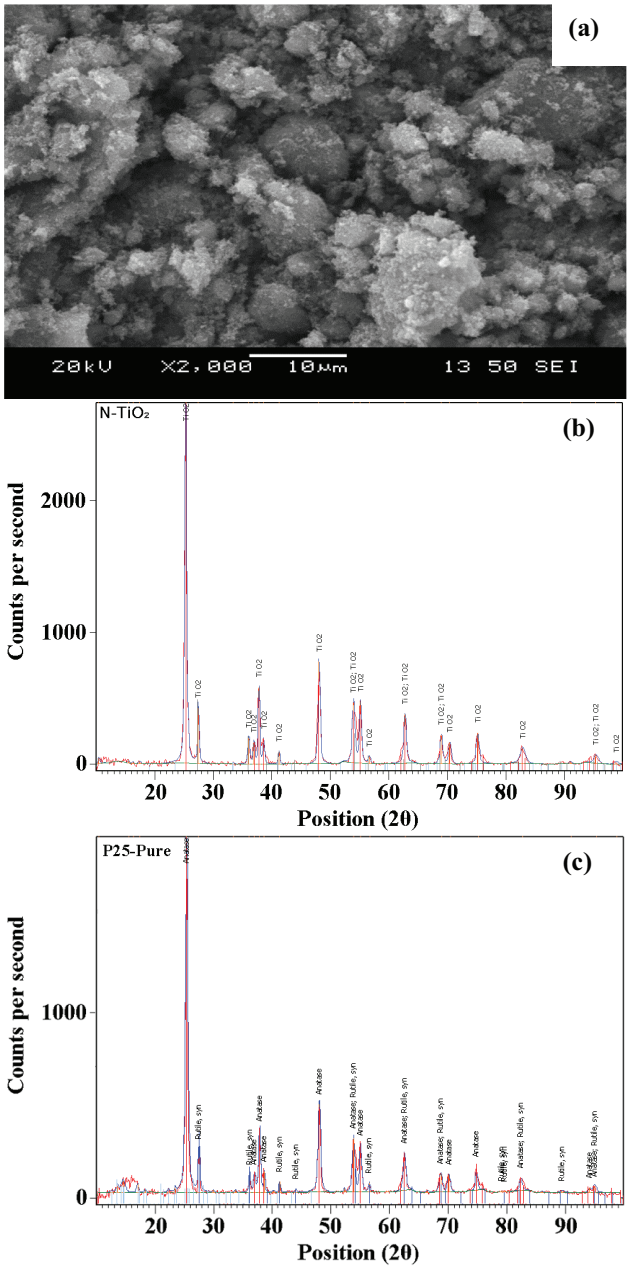

Fig. 3. (a) SEM image of the as-prepared N-TiO_2 photocatalyst (0.15 w:w N-TiO_2) by the annealing method; diffractogram (XRD) of the (b) as-prepared N-TiO_2 photocatalyst; and (c) P25-Pure.

of pure P25 and N-TiO_2 are in the same position. It can be concluded that nitrogen is a part of the crystal lattice of TiO_2 due to the relatively same size of oxygen and nitrogen [41]. It seems that a crystal defect took place and that is why the photocatalytic activity of the N-TiO_2 is enhanced.

Fig. 4 comprises four mapping images of the N-doped TiO_2 0.15 w:w N-TiO_2 photocatalyst prepared by annealing technique. Fig. 4(a) illustrates the whole sample of N-TiO_2 while Figs. 4(b)–(d) show images of the titanium, oxygen, and nitrogen elements ejected from Kα (the most intense peak) shells of each atom in the photocatalyst, respectively. The mapping image confirmed that the N-doped TiO_2 photocatalyst comprises nitrogen, as a dopant, in the structure of the N-TiO_2 composite.

3.3. Statistical analysis and optimization studies

Table 2 presents the four-factor BBD with experimental and predicted values for both the percent TOC and color removals by the developed quadratic statistical models for the degradation of methyl orange by photocatalysis using the N-TiO_2 (0.15 w:w N-TiO_2) in a laboratory-scale slurry batch photoreactor. The RSM was used to indicate the relationship between the predictors and the process responses. Hence, to predict the response functions for both the TOC removal (Y_1) and the color removal (Y_2), Eqs. (4) and (5) were developed in terms of the coded factors, respectively:

$$Y_1 = 57.02 - 11.62X_1 - 18.87X_2 + 3.49X_3 - 3.74X_4 - 15.11X_1X_2 - 0.01X_1X_3 - 0.99X_1X_4 - 12.56X_2X_3 + 6.49X_2X_4 - 5.86X_3X_4 + 1.75X_1^2 - 0.33X_2^2 - 4.44X_3^2 - 8.48X_4^2 \quad (4)$$

$$Y_2 = 40.62 - 7.10X_1 - 16.01X_2 + 9.97X_3 - 4.46X_4 + 16.25X_1X_2 - 5.68X_1X_3 + 3.25X_1X_4 - 9.14X_2X_3 + 4.54X_2X_4 - 9.29X_3X_4 + 0.28X_1^2 + 4.96X_2^2 + 9.22X_3^2 + 1.20X_4^2 \quad (5)$$

The evaluation of the signs of the coefficients offers quick scrutiny of the parametrical effects of the model variables on the responses. Negative coefficients point out unfavorable effects on both the percent TOC and color removals for the model components X_1, X_2, X_4, X_1X_2, X_1X_3, X_1X_4, X_2X_3, X_3X_4, X_2^2, X_3^2, and X_4^2 in Y_1 and X_1, X_2, X_4, X_1X_3, X_2X_3, and X_3X_4 in Y_2.

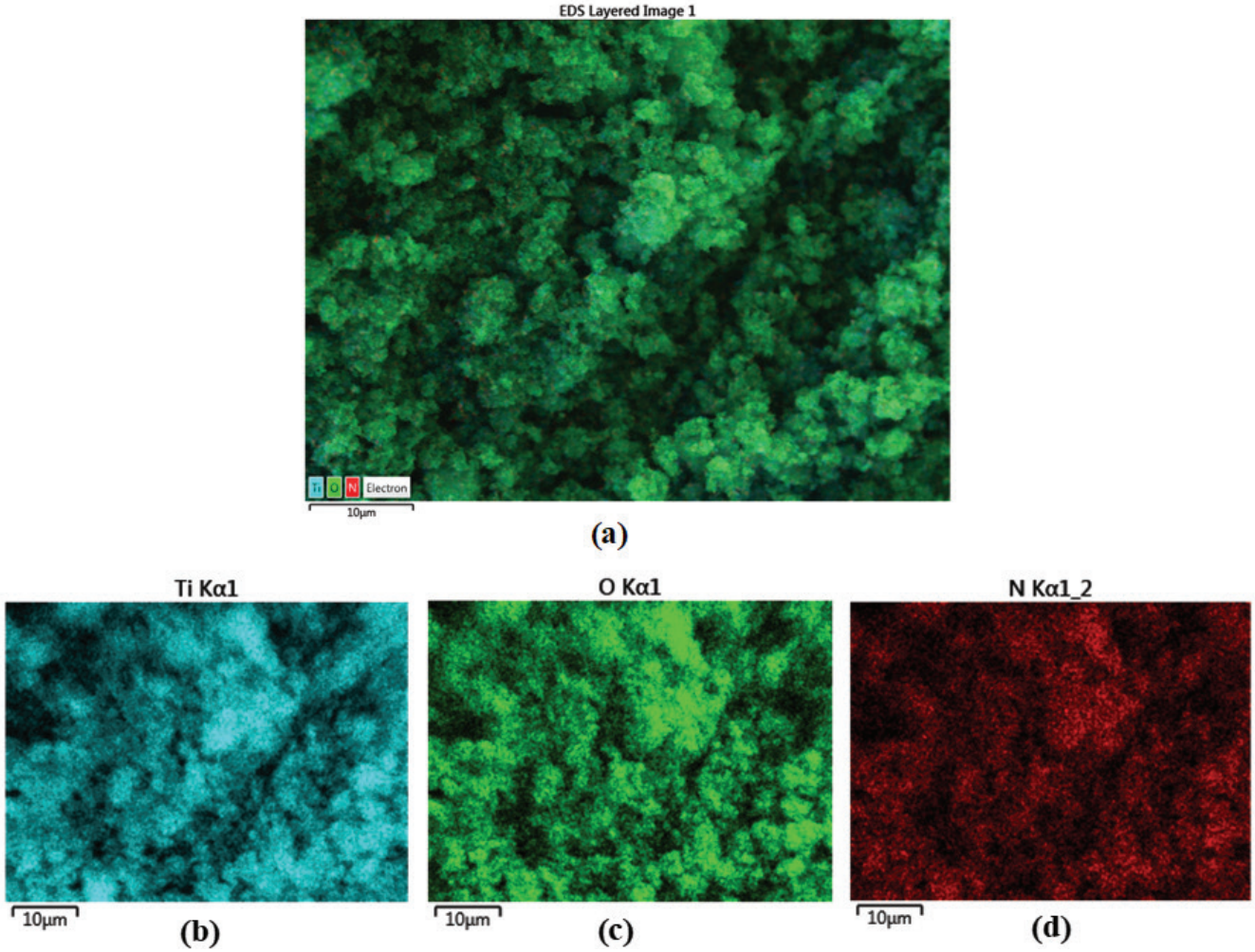

Fig. 4. Mapping images of (a) N-TiO_2 (0.15 w:w N-TiO_2) photocatalyst along with the elemental distribution of (b) titanium; (c) oxygen; and (d) nitrogen, in the photocatalyst prepared by annealing method.

Table 2
Four-factor BBD for RSM, along with the observed and predicted percent TOC and color removals in the optimization of the photocatalytic activity of N-doped TiO_2 for the degradation of an azo dye

Run	Independent coded variables				TOC removal (%)		Color removal (%)	
	X_1	X_2	X_3	X_4	Observed	Predicted	Observed	Predicted
1	–1	–1	0	0	72.64	73.82	84.50	85.21
2	1	–1	0	0	81.86	80.81	37.85	38.53
3	–1	1	0	0	65.81	66.30	21.31	20.70
4	1	1	0	0	14.59	12.85	39.65	39.00
5	0	0	–1	–1	38.91	38.49	39.04	36.24
6	0	0	1	–1	58.28	57.19	73.84	74.76
7	0	0	–1	1	42.20	42.73	46.75	45.89
8	0	0	1	1	38.14	38.00	44.40	47.27
9	–1	0	0	–1	64.77	64.66	53.46	56.90
10	1	0	0	–1	42.70	43.41	38.57	36.21
11	–1	0	0	1	59.56	59.16	38.71	41.48
12	1	0	0	1	33.53	33.95	36.82	33.79
13	0	–1	–1	0	54.08	55.07	49.33	51.70
14	0	1	–1	0	42.35	42.45	37.98	37.95
15	0	–1	1	0	86.97	87.18	89.48	89.92
16	0	1	1	0	24.99	24.31	41.58	39.63
17	–1	0	–1	0	63.75	62.44	43.81	41.55
18	1	0	–1	0	39.12	39.23	35.15	38.73
19	–1	0	1	0	69.31	69.45	76.92	72.86
20	1	0	1	0	44.63	46.19	45.53	47.31
21	0	–1	0	–1	77.65	77.31	73.26	71.80
22	0	1	0	–1	25.36	26.60	28.44	30.70
23	0	–1	0	1	57.85	56.86	56.53	53.79
24	0	1	0	1	31.50	32.09	29.87	30.85
25	0	0	0	0	57.79	57.02	40.27	40.62
26	0	0	0	0	54.18	57.02	46.80	40.62
27	0	0	0	0	54.12	57.02	43.60	40.62
28	0	0	0	0	58.98	57.02	37.35	40.62
29	0	0	0	0	57.18	57.02	40.43	40.62
30	0	0	0	0	59.87	57.02	35.27	40.62

Positive coefficients refer to favorable effects on both the percent TOC and color removals for the model components X_3, X_2X_4, and X_1^2 in Y_1 and X_3, X_1X_2, X_1X_4, X_2X_4, X_1^2, X_2^2, X_3^2, and X_4^2 in Y_2. Factors with coefficient values close to zero indicate a lower relative intensity than those above. Thus, X_1X_3, X_1X_4, X_1^2, and X_2^2 do not strongly affect the percent TOC removal while X_1^2 and X_4^2 do not intensely affect the percent color removal. The statistical significance of the developed models and predictors was further evaluated using the ANOVA with 95% confidence intervals for the percent TOC and color removals as shown in Tables 3 and 4, respectively.

The statistical significance of each factor coefficient was determined by the Fisher's (F) exact test, using probability (p) values. As shown in Tables 3 and 4, the F values 202.96 and 41.13 for the developed models related to percent TOC and color removals, respectively, indicate the significance of the models. Moreover, low probability values ($p < 0.05$) imply the significance of the model variables while confirming the model accuracy. On the other hand, p values higher than 0.10 imply the model variables are not significant. In this study, X_1X_3, X_1X_4, and X_2^2 are not significant for the removal of TOC while X_1X_4, X_1^2, and X_4^2 are not significant for color removal.

The goodness of fit for each model was validated using both the determination coefficient (R^2) and the adjusted R^2 to ensure a suitable variation of the model predictions to the observed values. The values of R^2 and adjusted R^2 reached 0.9947 and 0.9898 for the TOC removal and 0.9746 and 0.9509 for the color removal, respectively. Thus, high R^2 and adjusted R^2 values represent that the model is highly significant. The closer the values of R^2 and adjusted R^2 are to 1.0, the better the model prediction is [16,42].

Furthermore, the adequate precision of both the percent TOC and color removal models were found to be 60.03% (Table 3) and 26.61% (Table 4), respectively; thus, the models can be used to navigate the BBD space [16]. The lack of fit approach was also considered to measure how well the developed models fit the observed values. Accordingly, the p values of the lack of fit for the TOC and color removal models

were 0.9540 (Table 3) and 0.7227 (Table 4), respectively. An insignificant lack of fit ($p > 0.10$) is a desirable property because it suggests the models fit the data well.

The continuous variance assumption was confirmed graphically using the plot of predicted values vs. the internally studentized residuals (Fig. 5(a)), where the studentized residual values were obtained by dividing the residual values by their respective standard deviation.

Fig. 5(a) also shows randomly scattered points between the outlier detection limits from –3 to +3. Furthermore, the observed and predicted value correlations for both the percent TOC and color removals are presented in Fig. 5(b). A straight-line trend shows minor discrepancies and an agreement between predicted and experimental values. Therefore, the model predictions for both TOC removal, Eq. (4), and color removal, Eq. (5), are satisfactory.

3.4. Individual effect of model parameters

Since the significance of the TOC and color removal models (Tables 3 and 4, respectively) and the accuracy of the model predictions (Fig. 5) were confirmed, it was required to examine the significance of the model factors. This evaluation was performed using both the *F* exact test and *p* values, similar to the model significance evaluation, for each variable including linear, cross-factor, and quadratic interaction. As presented in Tables 3 and 4, model coefficients with *p* values lower than 0.05 are significant. Therefore, all four predictors, the light wavelength (X_1), the initial TOC concentration (X_2), the light intensity in terms of the number of lamps (X_3), and the pH (X_4), have significant effects on both responses, the TOC removal (Y_1) and the color removal (Y_2), based on their *p* value.

Fig. 6 illustrates the individual effect of the light wavelength, initial TOC concentration, light intensity, and pH on the percent TOC and color removals. It can be observed that both the light wavelength and the initial TOC concentration as they increase, both the percent TOC and color removals decrease. In the case of the light intensity, as the number of lamps increases, both the TOC and color removals rise to a point where there is no further increase in efficiency regardless of the number of lamps.

Conversely, results indicate an inversely proportional relationship of the light wavelength and initial TOC concentration with both the percent TOC and color removals. Therefore, the efficiency increases when the light spectrum is closest to the UV-C range with the peak at 254 nm and the lowest initial concentration of TOC. Finally, no pH adjustments are required to achieve maximum TOC and color removal efficiencies, as the maximum is located within the pH range of 6.5–7.5.

Table 3
ANOVA of percent TOC removal by quadratic modeling in the optimization of the photocatalytic activity of N-doped TiO_2 (0.15 w:w N-TiO_2) for the degradation of an azo dye

Source	Sum of squares	df[a]	Mean square	*F* Value[b]	*p* Value[c]	Remark
TOC model	8,713.4	14	622.39	202.96	<0.0001	Significant
X_1 = light wavelength	1,619.6	1	1,619.6	528.14	<0.0001	Significant
X_2 = TOC_o	4,273.3	1	4,273.3	1,393.5	<0.0001	Significant
X_3 = light intensity	146.37	1	146.37	47.731	<0.0001	Significant
X_4 = pH	167.93	1	167.93	54.760	<0.0001	Significant
X_1X_2	913.25	1	913.25	297.81	<0.0001	Significant
X_1X_3	0.0006	1	0.0006	0.0002	0.9888	Not significant
X_1X_4	3.9204	1	3.9204	1.2784	0.2759	Not significant
X_2X_3	631.27	1	631.27	205.85	<0.0001	Significant
X_2X_4	168.22	1	168.22	54.856	<0.0001	Significant
X_3X_4	137.24	1	137.24	44.754	<0.0001	Significant
X_1^2	21.020	1	21.020	6.8546	0.0194	Significant
X_2^2	0.7317	1	0.7317	0.2386	0.6323	Not significant
X_3^2	135.28	1	135.28	44.115	<0.0001	Significant
X_4^2	492.71	1	492.71	160.67	<0.0001	Significant
Residual	45.999	15	3.0666			
Lack of fit	16.940	10	1.6940	0.2915	0.9540	Not significant
Pure error	29.058	5	5.8116			
Corrected total SS[d]	8,759.4	29				
R^2	0.9947					
Adjusted R^2	0.9898					
Adequate precision	60.029					

[a]Degrees of freedom (df).
[b]Fisher's (*F*) exact test value.
[c]A probability value (p) < 0.05 is considered significant, a *p* value > 0.10 is considered not significant.
[d]Total sum of squares corrected for the mean.

Table 4
ANOVA of percent color removal by quadratic modeling in the optimization of the photocatalytic activity of N-doped TiO_2 (0.15 w:w N-TiO_2) for the degradation of an azo dye

Source	Sum of squares	df[a]	Mean square	*F* Value[b]	*p* Value[c]	Remark
Color model	7,794.0	14	556.72	41.13	<0.0001	Significant
X_1 = light wavelength	604.07	1	604.07	44.63	<0.0001	Significant
X_2 = TOC_o	3,075.8	1	3,075.8	227.2	<0.0001	Significant
X_3 = light intensity	1,193.8	1	1,193.8	88.201	<0.0001	Significant
X_4 = pH	238.79	1	238.79	17.642	0.0008	Significant
X_1X_2	1,055.9	1	1,055.9	78.01	<0.0001	Significant
X_1X_3	129.16	1	129.16	9.5428	0.0075	Significant
X_1X_4	42.250	1	42.250	3.1215	0.0976	Not significant
X_2X_3	333.98	1	333.98	24.67	0.0002	Significant
X_2X_4	82.446	1	82.446	6.091	0.0261	Significant
X_3X_4	345.03	1	345.03	25.492	0.0001	Significant
X_1^2	0.5217	1	0.5217	0.0385	0.8470	Not significant
X_2^2	168.92	1	168.92	12.4804	0.0030	Significant
X_3^2	582.55	1	582.55	43.040	<0.0001	Significant
X_4^2	9.9086	1	9.9086	0.73	0.4057	Not significant
Residual	203.03	15	13.535			
Lack of fit	116.48	10	11.648	0.6729	0.7227	Not significant
Pure error	86.547	5	17.309			
Corrected total SS[d]	7,997.1	29				
R^2	0.9746					
Adjusted R^2	0.9509					
Adequate precision	26.610					

[a]Degrees of freedom (df).
[b]Fisher's (*F*) exact test value.
[c]A probability value (p) < 0.05 is considered significant, a p value > 0.10 is considered not significant.
[d]Total sum of squares corrected for the mean.

3.5. Interaction of model parameters, 2D contour plots, and 3D response surface

As shown in Tables 3 and 4, among all model parameters, only the interaction between the light wavelength and pH (X_1X_4) did not indicate a significant effect on both the percent TOC and color removals. Additionally, the interaction between the light wavelength and the light intensity (X_1X_3) did not show a significant effect on the percent TOC removal while being significant on the color removal. In contrast, the cross-factor interaction between the light wavelength and the initial TOC concentration (X_1X_2) and those of the light intensity with the initial TOC concentration (X_2X_3) and the pH (X_3X_4) were found to have a very high significant effect on both TOC and color removals.

The cross-factor interaction effects between independent factors were plotted into the 3D surfaces and 2D contour plots shown in Figs. 7 and 8 for the removal of TOC and color, respectively, representing the graphical regression analysis; thus, the response functions of the variation and interaction of two predictors are presented while all other factors are fixed at the center levels [13–16].

Figs. 7 and 8(a)–(c) depict the effects of the light wavelength on the percent TOC and color removals. Results show that by decreasing the wavelength, both the percent TOC and color removal increase. In all cases, the light intensity and initial TOC concentration cross-factor interactions with the light wavelength are intensified when the latter is at the lowest range value while pH does not require adjustments (Figs. 7(c) and 8(c)). The interaction of the initial TOC concentration with other independent variables tends to intensify their effect at low levels confirmed in Figs. 7 and 8(a), (d), and (e) as expected.

On the other hand, as shown in Figs. 7 and 8(b), (d), and (f), both the percent TOC and color removals increase by increasing the light intensity in terms of the number of lamps. The effect of the light intensity on both the percent TOC and color removals is mainly attributable to the absorption of the UV radiation by organic compounds along with intermediates formed during the photocatalytic reactions, which as the light intensity increases there is a more uniform radiation distribution within the photoreactor. This effect is intensified at a lower light wavelength due to the photoactivity of the composite N-TiO_2 photocatalyst (Figs. 7(b) and 8(b)) and at low initial concentration of TOC (Figs. 7(d) and 8(d)) while being slight while interacting with the pH (Figs. 7(f) and 8(f)), which results in an adequate value for each parameter within the range in terms of optimization potential.

Lastly, Figs. 7 and 8(c), (e), and (f) depict the interaction effects of the pH with other variables, including the light wavelength (X_1X_4), the initial TOC concentration (X_2X_4), and the light intensity (X_3X_4) on the percent TOC and color removals. Results demonstrate that there is no need for further pH

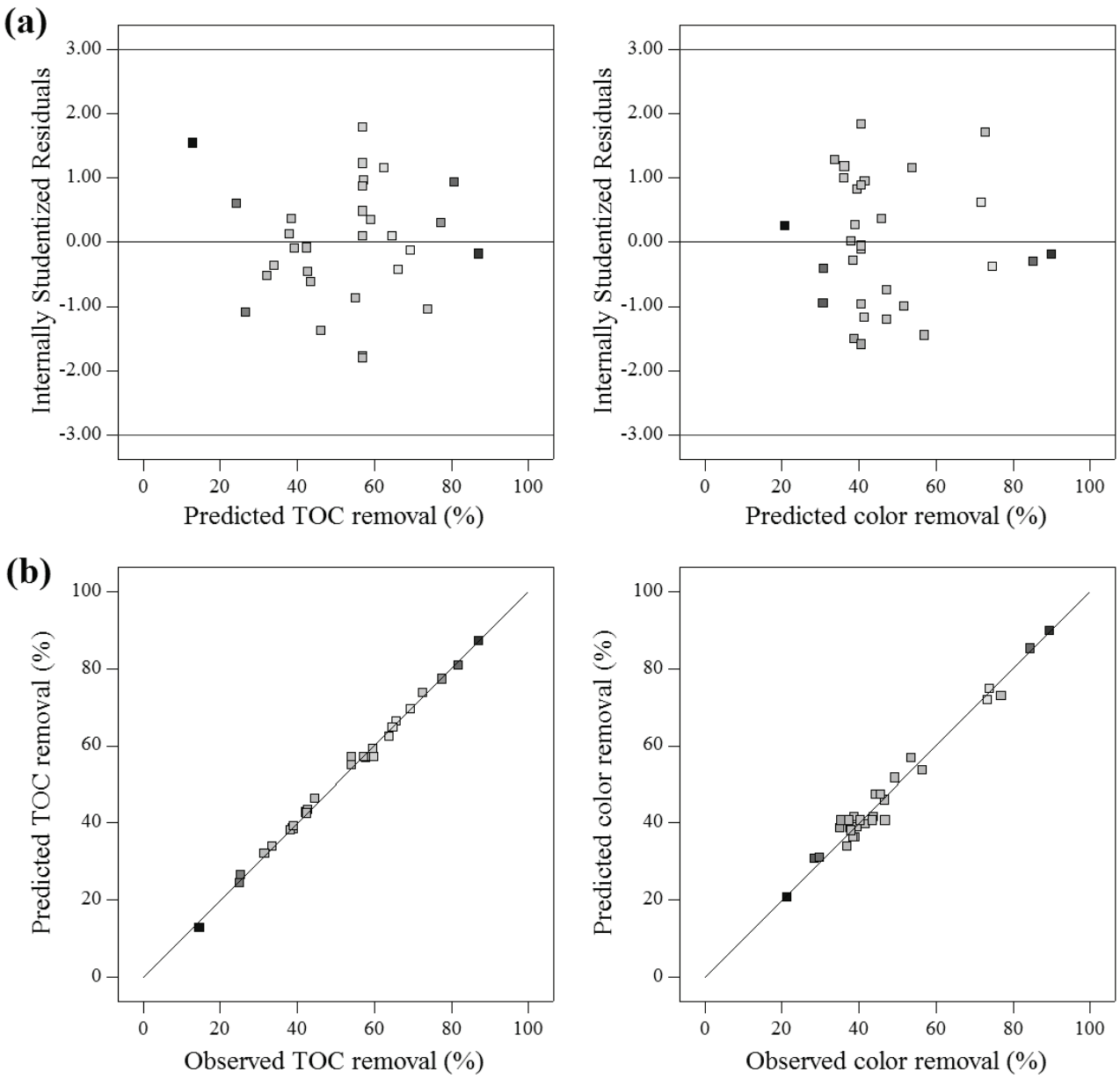

Fig. 5. Validation of the percent TOC removal (left side) and color removal (right side) models using different plots: (a) internally studentized residuals vs. predicted values; (b) observed experimental data vs. predicted values.

adjustments. These interactions also confirm that both the percent TOC and color removals are directly proportional to the light intensity while being inversely proportional to the light wavelength and initial TOC concentration, and confirms there is no need for pH adjustment.

3.6. Optimization of experimental conditions and process parameters

The RSM was used to determine the optimal experimental conditions of the four predictors, including the light wavelength (X_1), the initial TOC concentration (X_2), the light intensity in terms of the number of lamps (X_3), and the pH (X_4), to obtain the maximum percent TOC removal (Y_1) and color removal (Y_2).

The optimization was accomplished by maximizing both the percent TOC and color removals at defined operating conditions using the numerical optimization method built into the statistical software Design-Expert 10.0.3.1. Both Eqs. (4) and (5) were used as the objective functions for the percent TOC and color removals, respectively, while the independent variables were used as constraints in their critical ranges.

The numerical optimization explores the BBD space using the developed statistical models to find the optimal operating conditions that meet the set goal of optimization for maximum TOC and color removals simultaneously.

The multiple-response function shown in Eq. (3) was used to obtain the parameter interaction plots, as depicted in Fig. 9, by maximizing the TOC removal (Y_1) and color

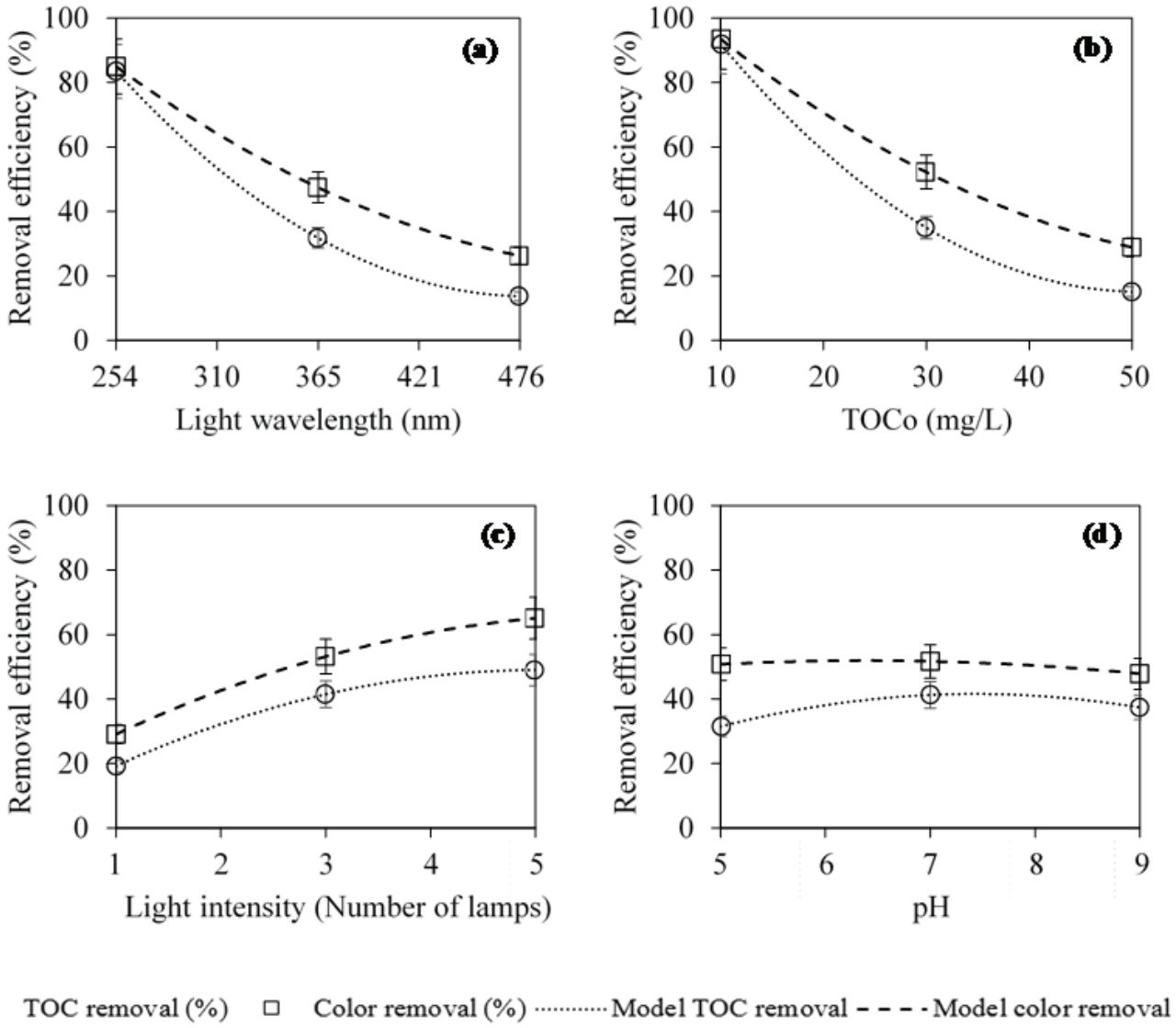

Fig. 6. Individual effect of the (a) light wavelength; (b) initial TOC concentration; (c) light intensity; and (d) pH on the percent TOC and color removals using 0.15 w:w N-TiO_2. The dashed lines represent model predicted values, whereas the marker points represent the experimental values. Error bars represent the standard deviation of the experimental data.

removal (Y_2) by the numerical optimization using the optimum factor settings. Therefore, the desirability value of 1.00 was found for achieving the maximum TOC and color removals of 96.11% and 98.18%, respectively, at the optimum conditions of light intensity in terms of five lamps, light wavelength of 418 nm (visible light range), initial TOC concentration of 10.54 mg/L, and pH of 6.66 for the photocatalytic treatment of azo dyes in aqueous solution using the composite N-TiO_2 photocatalyst.

As a final confirmation, the obtained optimum experimental conditions were tested in another experiment to validate the response values. Consequently, the TOC removal of 96.11% and the color removal of 98.18% were obtained experimentally, confirming the reliability and accuracy of the developed models since they both are between the 95% CI of 92%–100% for TOC removal and 83%–100% for color removal.

4. Conclusions

The RSM combined with a four-factor BBD revealed reliable results for the treatment of azo dyes in aqueous solution by photocatalysis in a batch reactor using the composite N-TiO_2 photocatalyst. The accuracy of the developed quadratic models was evaluated using ANOVA. The cross-factor interaction between the light wavelength and the light intensity presented a significant effect on the color removal while being not significant on the TOC removal. Meanwhile, the interaction effect between light wavelength and pH was found not significant on both the TOC and color removal efficiencies. In contrast, the cross-factor interaction between the light wavelength and the initial TOC concentration and those of the light intensity with the initial TOC concentration and the pH were found to have highly significant effects on both TOC and color removals for the photocatalytic treatment of azo dyes to minimize treatment-related costs.

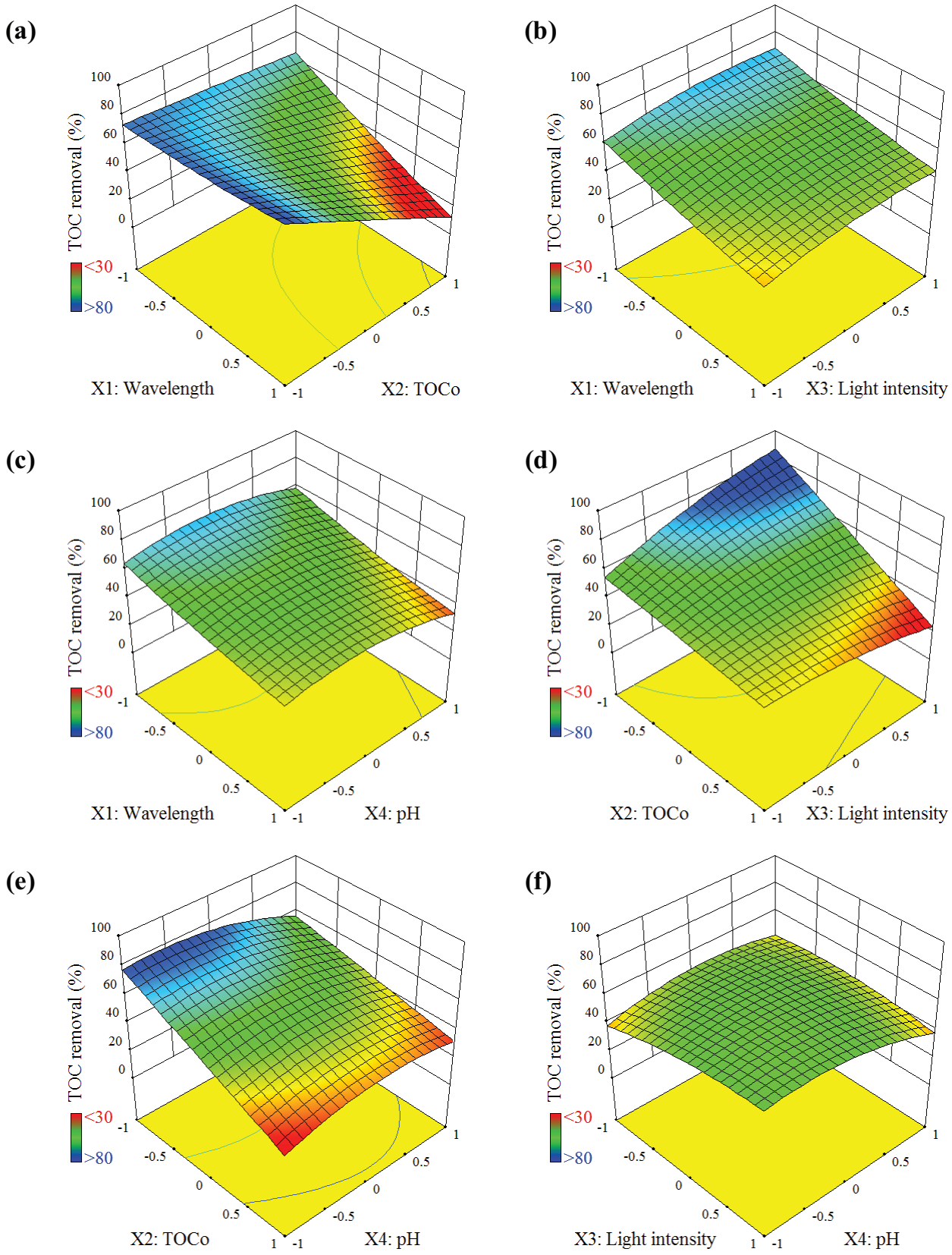

Fig. 7. Interaction effects of different parameters on the percent TOC removal using 3D response surface and 2D contours: (a) light wavelength and initial TOC concentration (X_1X_2); (b) light wavelength and intensity (X_1X_3); (c) light wavelength and pH (X_1X_4); (d) initial TOC concentration and light intensity (X_2X_3); (e) initial TOC concentration and pH (X_2X_4); and (f) light intensity and pH (X_3X_4).

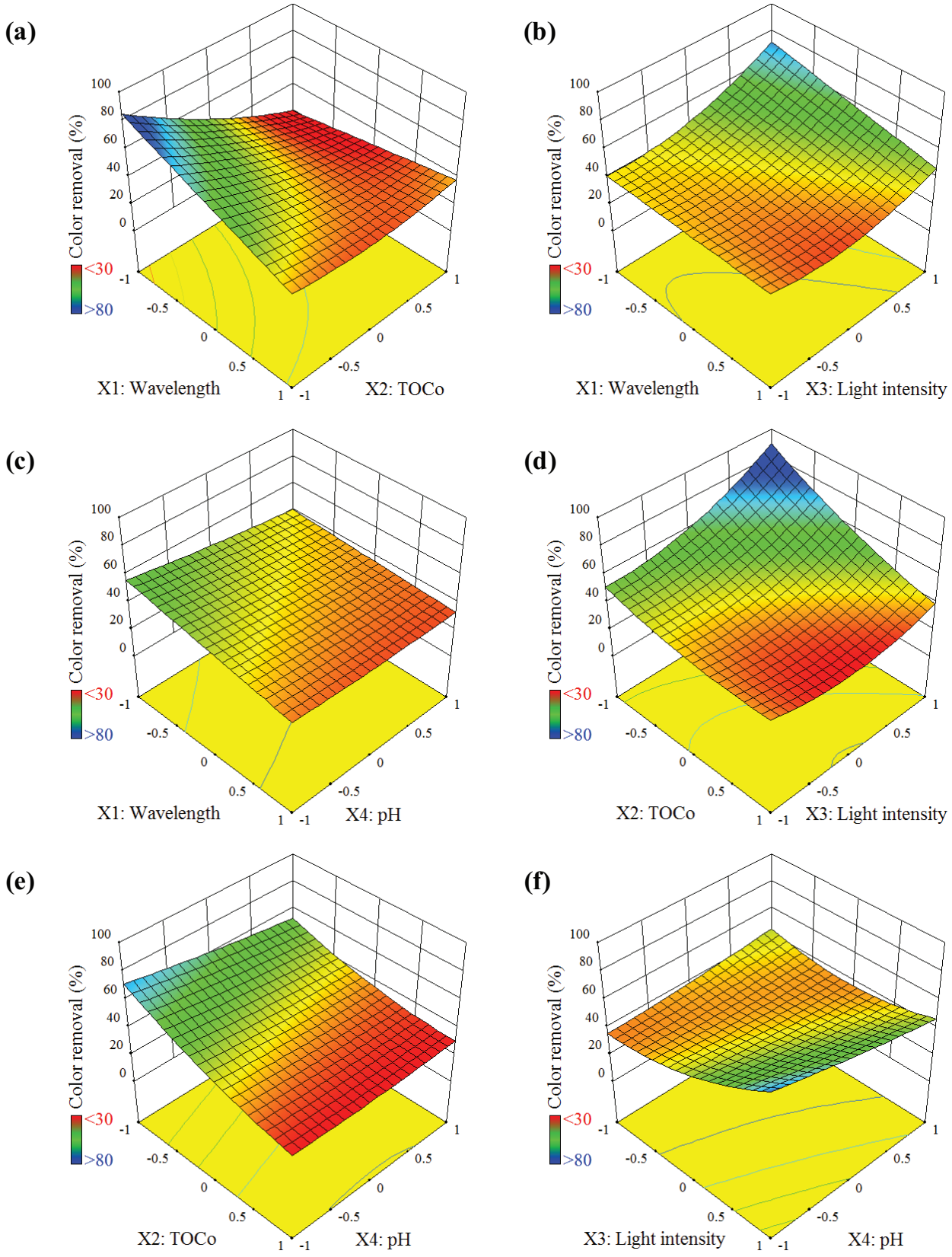

Fig. 8. Interaction effects of different parameters on the percent color removal using 3D response surface and 2D contours: (a) light wavelength and initial TOC concentration (X_1X_2); (b) light wavelength and intensity (X_1X_3); (c) light wavelength and pH (X_1X_4); (d) initial TOC concentration and light intensity (X_2X_3); (e) initial TOC concentration and pH (X_2X_4); and (f) light intensity and pH (X_3X_4).

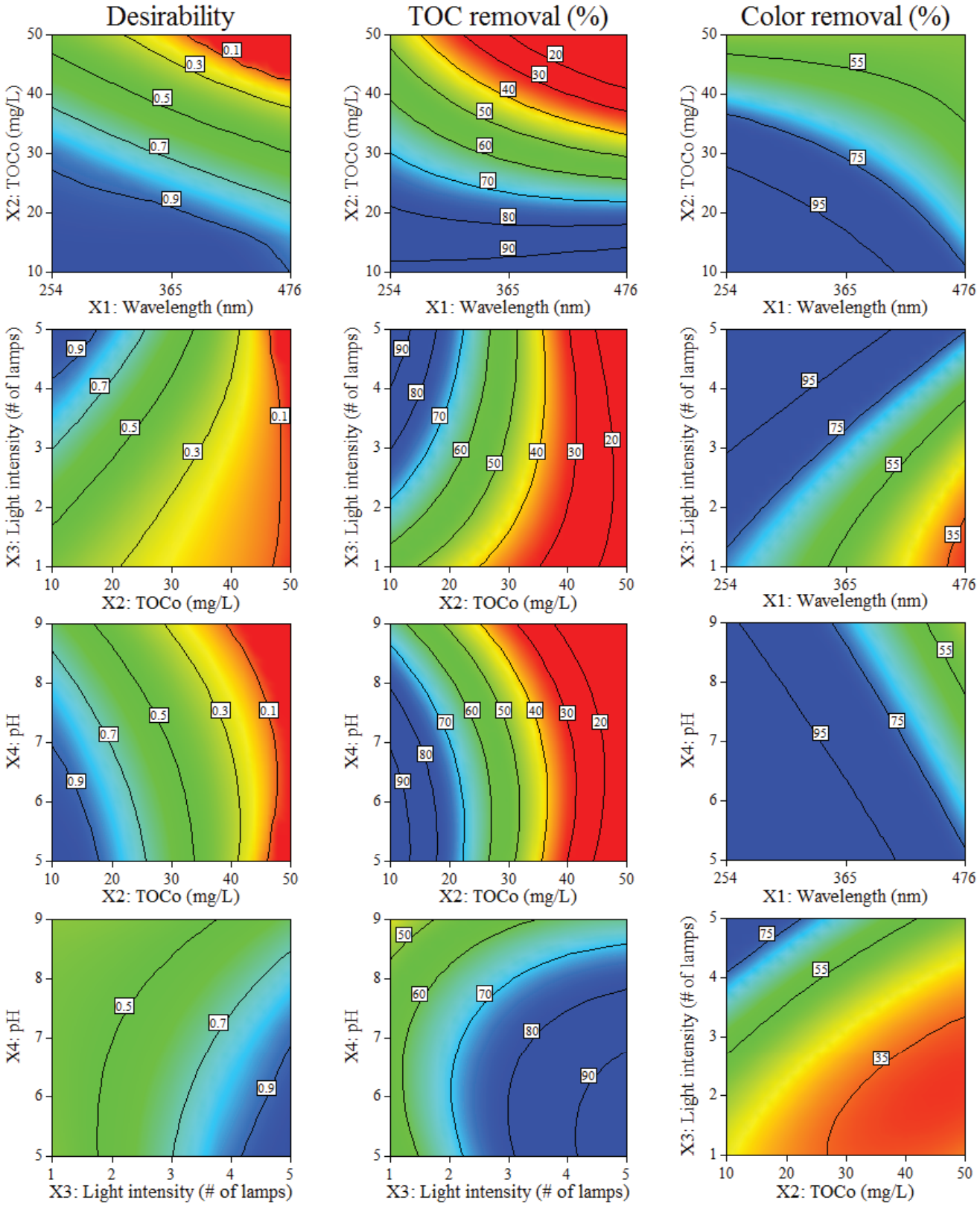

Fig. 9. Desirability 2D plots maximizing the percent TOC and color removals at optimum factor settings of light intensity in terms of five lamps, light wavelength of 418 nm (visible light range), initial TOC concentration of 10.54 mg/L, and pH of 6.66 for the photocatalytic treatment of azo dyes in aqueous solution using the composite N-TiO_2 photocatalyst.

Maximum TOC and color removal efficiencies of 96.11% and 98.18%, respectively, were achieved at the optimum operating conditions of light intensity in terms of five lamps, light wavelength of 418 nm (visible light range), initial TOC concentration of 10.54 mg/L, and pH of 6.66 based on the developed quadratic models and the desirability multiple-response method. For the maximum TOC and color removal based on DOE, the best results were obtained by visible irradiation, confirming that the light absorption was extended to a higher wavelength along with a red shift in the application of N-TiO_2 photocatalyst.

The developed statistical models presented a detailed examination of the simultaneous interaction effects of the predictors on the model responses. Therefore, the proposed statistical models could successfully describe the degradation of azo dyes by photocatalysis using the N-doped TiO_2 composite under visible light and could be utilized as a base for future research on photoreactor design, process optimization, and scale-up studies.

Acknowledgments

The financial support of Natural Sciences and Engineering Research Council of Canada (NSERC), Ontario Graduate Scholarship (OGS), and Ryerson University Faculty of Engineering and Architectural Science Dean's Research Fund is much appreciated.

References

[1] U.G. Akpan, B.H. Hameed, Parameters affecting the photocatalytic degradation of dyes using TiO_2-based photocatalysts: a review, J. Hazard. Mater., 170 (2009) 520–529.
[2] M. Visa, F. Pricop, A. Duta, Sustainable treatment of wastewaters resulted in the textile dyeing industry, Clean Technol. Environ. Policy, 13 (2011) 855–861.
[3] F.V. De Andrade, G.M. De Lima, R. Augusti, M.G. Coelh, J.D. Ardisson, O.B. Romero, A versatile approach to treat aqueous residues of textile industry: the photocatalytic degradation of Indigo Carmine dye employing the autoclaved cellular concrete/Fe_2O_3 system, Chem. Eng. J., 180 (2012) 25–31.
[4] A. Buthiyappan, A.R. Abdul Aziz, W.M.A. Wan Daud, Recent advances and prospects of catalytic advanced oxidation process in treating textile effluents, Rev. Chem. Eng., 32 (2016) 1–47.
[5] M. Nasirian, C.F. Bustillo-Lecompte, M. Mehrvar, Photocatalytic efficiency of Fe_2O_3/TiO_2 for the degradation of typical dyes in textile industries: effects of calcination temperature and UV-assisted thermal synthesis, J. Environ. Manage., 196 (2017) 487–498.
[6] M. Nasirian, M. Mehrvar, Modification of TiO_2 to enhance photocatalytic degradation of organics in aqueous solutions, J. Environ. Chem. Eng., 4 (2016) 4072–4082.
[7] X.L. Zou, Combination of ozonation, activated carbon, and biological aerated filter for advanced treatment of dyeing wastewater for reuse, Environ. Sci. Pollut. Res., 22 (2015) 8174–8181.
[8] M. Mohajerani, M. Mehrvar, F. Ein-Mozaffari, Correlation and prediction of azo dye degradation by nonlinear least-square regression in combined ozonation and ultrasonolysis processes, Water Qual. Res. J. Can., 46 (2011) 250–258.
[9] M. Mohajerani, M. Mehrvar, F. Ein-Mozaffari, Degradation of aqueous methylene blue using an external loop airlift sonophotoreactor: statistical analysis and optimization, J. Environ. Sci. Health, Part A, 51 (2016) 722–735.
[10] A. Mowla, M. Mehrvar, R. Dhib, Combination of sonophotolysis and aerobic activated sludge processes for treatment of synthetic pharmaceutical wastewater, Chem. Eng. J., 255 (2014) 411–423.
[11] C.F. Bustillo-Lecompte, M. Mehrvar, Slaughterhouse wastewater characteristics, treatment, and management in the meat processing industry: a review on trends and advances, J. Environ. Manage., 161 (2015) 287–302.
[12] D. Hamad, M. Mehrvar, R. Dhib, Experimental study of polyvinyl alcohol degradation in aqueous solution by UV/H_2O_2 process, Polym. Degrad. Stab., 103 (2014) 75–82.
[13] D. Hamad, R. Dhib, M. Mehrvar, Photochemical degradation of aqueous polyvinyl alcohol in a continuous UV/H_2O_2 process: experimental and statistical analysis, J. Polym. Environ., 24 (2016) 72–83.
[14] C.F. Bustillo-Lecompte, M. Mehrvar, Treatment of an actual slaughterhouse wastewater by integration of biological and advanced oxidation processes: modeling, optimization, and cost-effectiveness analysis, J. Environ. Manage., 182 (2016) 651–666.
[15] C. Bustillo-Lecompte, M. Mehrvar, E. Quiñones-Bolaños, Slaughterhouse wastewater characterization and treatment: an economic and public health necessity of the meat processing industry in Ontario, Canada, J. Geosci. Environ. Prot., 4 (2016) 175–186.
[16] C.F. Bustillo-Lecompte, S. Ghafoori, M. Mehrvar, Photochemical degradation of an actual slaughterhouse wastewater by continuous UV/H_2O_2 photoreactor with recycle, J. Environ. Chem. Eng., 4 (2016) 719–732.
[17] C.F. Bustillo-Lecompte, M. Mehrvar, E. Quiñones-Bolaños, Cost-effectiveness analysis of TOC removal from slaughterhouse wastewater using combined anaerobic-aerobic and UV/H_2O_2 processes, J. Environ. Manage., 134 (2014) 145–152.
[18] C.F. Bustillo-Lecompte, M. Knight, M. Mehrvar, Assessing the performance of UV/H_2O_2 as a pretreatment process in TOC removal of an actual petroleum refinery wastewater and its inhibitory effects on activated sludge, Can. J. Chem. Eng., 93 (2015) 798–807.
[19] K. Zhao, Z. Wu, R. Tang, Y. Jiang, Preparation of highly visible-light photocatalytic active N-doped TiO_2 microcuboids, J. Korean Chem. Soc., 57 (2013) 489–492.
[20] S.A. Ansari, M.M. Khan, M.O. Ansari, M.H. Cho, Nitrogen-doped titanium dioxide (N-doped TiO_2) for visible light photocatalysis, New J. Chem., 40 (2016) 3000–3009.
[21] P. Namkhang, W.J. An, W.N. Wang, K.S. Rane, P. Kongkachuichay, P. Biswas, Low temperature synthesis of N-doped TiO_2 nanocatalysts for photodegradation of methyl orange, J. Nanosci. Nanotechnol., 13 (2013) 2376–2381.
[22] F. Azizi, F. Molani, Effects of N doping on structure and improvement photocatalytic properties of anatase TiO_2 nanoparticles, J. Nanostruct., 6 (2016) 58–63.
[23] B. Lin, G. Yang, B. Yang, Y. Zhao, Construction of novel three dimensionally ordered macroporous carbon nitride for highly efficient photocatalytic activity, Appl. Catal., B, 198 (2016) 276–285.
[24] B. Lin, S. Chen, F. Dong, G. Yang, A ball-in-ball g-C_3N_4@SiO_2 nano-photoreactor for highly efficient H_2 generation and NO removal, Nanoscale, 9 (2017) 5273–5279.
[25] B. Lin, H. An, X. Yan, T. Zhang, J. Wei, G. Yang, Fish-scale structured g-C_3N_4 nanosheet with unusual spatial electron transfer property for high-efficiency photocatalytic hydrogen evolution, Appl. Catal., B, 210 (2017) 173–183.
[26] B. Lin, H. Li, H. An, W. Hao, J.J. Wei, Y. Dai, C. Ma, G. Yang, Preparation of 2D/2D g-C_3N_4 nanosheet@$ZnIn_2S_4$ nanoleaf heterojunctions with well-designed high-speed charge transfer nanochannels towards high-efficiency photocatalytic hydrogen evolution, Appl. Catal., B, 220 (2018) 542–552.
[27] C. Xue, H. An, X. Yan, J. Li, B. Yang, J. Wei, G. Yang, Spatial charge separation and transfer in ultrathin $CdIn_2S_4$/rGO nanosheet arrays decorated by ZnS quantum dots for efficient visible-light-driven hydrogen evolution, Nano Energy, 39 (2017) 513–523.
[28] C. Xue, X. Yan, H. An, H. Li, J. Wei, G. Yang, Bonding CdS-Sn_2S_3 eutectic clusters on graphene nanosheets with unusually photoreaction-driven structural reconfiguration effect for excellent H_2 evolution and Cr(VI) reduction, Appl. Catal., B, 222 (2018) 157–166.

[29] A.A. Salarian, Z. Hami, N. Mirzaei, S.M. Mohseni, A. Asadi, H. Bahrami, M. Vosoughi, A. Alinejad, M.R. Zare, N-doped TiO_2 nanosheets for photocatalytic degradation and mineralization of diazinon under simulated solar irradiation: optimization and modeling using a response surface methodology, J. Mol. Liq., 220 (2016) 183–191.
[30] O. Sacco, M. Stoller, V. Vaiano, P. Ciambelli, A. Chianese, D. Sannino, Photocatalytic degradation of organic dyes under visible light on N-doped TiO_2 photocatalysts, Int. J. Photoenergy, 2012 (2012) 1–8.
[31] X. Wang, K. Zhang, X. Guo, G. Shen, J. Xiang, Synthesis and characterization of N-doped TiO_2 loaded onto activated carbon fiber with enhanced visible-light photocatalytic activity, New J. Chem., 38 (2014) 6139–6146.
[32] H.P. Shivaraju, N. Muzakkira, B. Shahmoradi, Photocatalytic treatment of oil and grease spills in wastewater using coated N-doped TiO_2 polyscales under sunlight as an alternative driving energy, Int. J. Environ. Sci. Technol., 13 (2016) 2293–2302.
[33] F. Veisi, M.A. Zazouli, M.A. Ebrahimzadeh, J.Y. Charati, A.S. Dezfoli, Photocatalytic degradation of furfural in aqueous solution by N-doped titanium dioxide nanoparticles, Environ. Sci. Pollut. Res., 23 (2016) 21846–21860.
[34] W. Shi, W. Yang, Q. Li, S. Gao, P. Shang, J.K. Shang, The synthesis of nitrogen/sulfur co-doped TiO_2 nanocrystals with a high specific surface area and a high percentage of {001} facets and their enhanced visible-light photocatalytic performance, Nanoscale Res. Lett., 7 (2012) 1–9.
[35] R.H. Myers, D.C. Montgomery, G.G. Vining, C.M. Borror, S.M. Kowalski, Response surface methodology: a retrospective and literature survey, J. Qual. Technol., 36 (2004) 53–77.
[36] J. Lynch, C. Giannini, J.K. Cooper, A. Loiudice, I.D. Sharp, R. Buonsanti, Substitutional or interstitial site selective nitrogen doping in TiO_2 nanostructures, J. Phys. Chem. C, 119 (2015) 7443–7452.
[37] H. Xu, S. Ouyang, L. Liu, P. Reunchan, N. Umezawa, J. Ye, Recent advances in TiO_2-based photocatalysis, J. Mater. Chem. A, 2 (2014) 12642–12661.
[38] A. Zaleska, Doped-TiO_2: a review, Recent Pat. Eng., 2 (2008) 157–164.
[39] A. Nikhil, G.S. Anjusree, S.V. Nair, A.S. Nair, Visible light-induced photocatalytic activity of high surface area N-doped two-dimensional (2-D) TiO_2 sheets, RSC Adv., 5 (2015) 88464–88470.
[40] S. Dai, Y. Wu, T. Sakai, Z. Du, H. Sakai, M. Abe, Preparation of highly crystalline TiO_2 nanostructures by acid-assisted hydrothermal treatment of hexagonal-structured nanocrystalline titania/cetyltrimethyammonium bromide nanoskeleton, Nanoscale Res. Lett., 5 (2010) 1829–1835.
[41] R. Asahi, T. Morikawa, T. Ohwaki, K. Aoki, Y. Taga, Visible-light photocatalysis in nitrogen-doped titanium oxides, Science, 293 (2001) 269–271.
[42] G.E. Botha, J.C. Oliveira, L. Ahrné, Quality optimisation of combined osmotic dehydration and microwave assisted air drying of pineapple using constant power emission, Food Bioprod. Process., 90 (2012) 171–179.